Journal of Applied Polymer Science

Evaluating the state of dispersion on cellulosic biopolymer by rheology

Tapasi Mukherjee, Nhol Kao, Rahul K. Gupta, Nurul Quazi, Sati Bhattacharya
Department of Chemical Engineering, Rheology and Materials Processing Centre, School of Civil, Environmental and Chemical Engineering, RMIT University, Melbourne Victoria 3001, Australia
Correspondence to: T. Mukherjee (E-mail: t.mukherjee@uq.edu.au)

ABSTRACT: The key challenge in the development of cellulose bio-nanocomposites lies in the spatial distribution of the cellulose fibre, as the presence of surface hydroxyl groups initiates self-agglomeration, thereby resulting in crack or failure of the composites. In this study, nanocrystalline cellulose (NCC) is here effectively surface acetylated to reduce agglomeration. Poly(lactic acid) PLA based cellulose bio- nanocomposites were then prepared by solvent casting technique. A rheological percolation threshold is calculated to quantify the level of dispersion and the optimal loading. Moreover, high frequency linear viscoelastic behavior is analyzed and the data is fitted to the Krieger-Dougherty equation to determine the maximum packing fraction. Maximum packing fraction value is then used as a mean to rank the quality of dispersion. The value for maximum packing fraction is compared with microcrystalline cellulose (MCC) and nanofibrillated cellulose (NFC), to show how shape and structure affects the quality of dispersion. © 2015 Wiley Periodicals, Inc. J. Appl. Polym. Sci. **2016**, *133*, 43200.

KEYWORDS: biomaterials; biopolymers and renewable polymers; cellulose and other wood products; rheology; surfaces and interfaces

Received 24 June 2015; accepted 2 November 2015
DOI: 10.1002/app.43200

INTRODUCTION

Development of cellulosic biopolymer is an active area of research over the last decade.[1–7] Some of the attractive features that explain its meaningful improvement as a reinforcing filler include its high aspect ratio,[8] their high crystallinity degree,[9] and high Young's modulus.[10,11] Cellulose as a filler is well known to set up an entangled network held through strong hydrogen bonding.[12] The key challenge in the development of such biocomposites lies in the control of the particulate structure, i.e., the spatial distribution of the cellulose fibre in a completely dispersed and stable state. Similar to other nanocomposite research, filler size, loading, and distribution dictate the amount of affected polymer, while the surface structure and chemistry of the particles dictate the intensity of interaction of the particle/polymer interphase. Literature review in this area clearly demonstrates that optimum performance requires an effective distribution of the nanoparticles within the matrix. However, dispersion of the nanofiller restricts the formation of interface, which makes the nanoparticle as an attractive choice for reinforcement. These particles have natural tendency to "stick" together and are difficult to separate or disperse due to high specific surface area and energy.[13] There is a constant citation by the review articles, referring to the challenges involved in nanoparticle distribution for the advancement of polymer nanocomposite technology.[14,15] Despite the broadly recognized importance of nanoparticle dispersion, the characterization of dispersion remains largely qualitative and mostly based on subjective interpretations of standard optical and electron microscopy images.

Rheology potentially offers a mean to assess the state of dispersion of nanocomposites directly in the melt state. The rheological properties, both linear and nonlinear ones, are sensitive to changes in the particulate microstructure, particle size, shape and surface characteristics of the dispersed phase, integrated over length scales.[26] The level of linear properties such as the storage and loss moduli, $G'$and G'', are always raised with filler addition. G' and G'' curves can be used diagnostically to assess the state of dispersion, since a flocculated system will show up as an extra low G' plateau. This usually takes the form of a progressive increase in the level of properties as more filler is added. However, sometimes, a secondary mechanism can be seen such as the development of a plateau usually from a pseudo network set up between flocs or chains of particles.[16]

Different approaches have been proposed to describe the dispersion quality of the polymer nanocomposites by linear viscoelastic behavior. Establishment of the power law relationship between elastic property and volume fraction assuming filler as the fractal aggregate is very popular.[17–19] The basic concept of the scaling theory for polymer gels is to relate the elastic

properties of a gel to its network structure. Near the gel point, the shear modulus of a gel behaves like $G' \sim (\varnothing\text{-}\varnothing_g)^t$ which is characteristic of a percolation transition. The theory also enables one to extract from the rheological measurements the structural information such as the fractal dimension of the individual flocs and the fractal dimension of the elastic backbones of the flocs.

Further to the study, changes to the high frequency moduli can also be considered as a mean to assess the dispersion quality, as they enable one to determine the effective hydrodynamic volume of the particles and aggregate over the entire range of volume fractions. At the highest frequencies probed, the polymer matrix contribution dominates over the aggregate contribution. At these frequencies, with increasing volume fraction, the moduli are observed to increase, which can be attributed to an increased effective deformation rate in the matrix. The higher moduli stem from an increase of the matrix contribution due to the hydrodynamic contribution. This can also be used to obtain information about the dispersion quality. In fact, from a methodological point of view, an interesting point is that high frequency data are easier to obtain and might provide a fast route to characterize dispersion. Here the volume occupied by aggregates is probed, even when they are part of a network. The relative high frequency moduli can be obtained by dividing the moduli by the values for the matrix. Further to the analysis, the evolution of the high relative frequency moduli can be described by the Krieger-Dougherty equation[20]:

$$G'_{HF,rel} = \frac{G'_{HF}}{G'_{HF,m}} = \left[1 - \frac{\varnothing}{\varnothing_{\max}}\right]^{-[\eta]\varnothing_{\max}} \quad \text{(i)}$$

Where $G'_{HF,rel}$ refers to the high frequency modulus of the nanocomposite, $G'_{HF,m}$ is the high frequency modulus of the matrix at the same frequency, $\varnothing$ is the volume fraction, $\varnothing_{\max}$ is the maximum packing fraction, and $[\eta]$ is the intrinsic viscosity. Typically for clay based nanocomposites, more exfoliation means lower $\varnothing_{\max}$.

The primary motivation behind this study is to evaluate the state of dispersion of acetylated nanocrystalline cellulose (NCC) in Polylactic Acid (PLA) based biopolymer using rheology. In earlier study, it has already been shown that surface acetylation of microcrystalline cellulose improves the degree of dispersion of the filler by arresting agglomeration.[21] In the previous study it was also observed that MCC acts more like a nanofiller, rather than a microfiller (the percolation reached at 2.5 wt %). Keeping the previous results in mind, MCC is acid hydrolyzed to produce NCC for effective nanoreinforcement. Similar surface acetylation on another variety of nanocellulose as regenerated from wood fiber, referred to as nanofibrillated cellulose (NFC), will be performed and the composites made from this filler will be compared to that of AC-NCC and AC-MCC (from previous study). A comparative analysis will be performed to rank the quality of dispersion from different varieties of nanocellulose, to show the correlation with native shape size and crystalline forms of nanocellulose to their dispersion quality.

EXPERIMENTAL

Nanocellulose was prepared by acid hydrolysis. Surface acetylation of nanocellulose has been carried out to prepare acetylated nanocellulose-based PLA composites. The composites were then characterized to confirm surface acetylation. Morphological characterization, to observe nanofibrill distribution in the PLA matrix, and measurement of the rheological properties of the composites has also been carried out. More specific details of the materials, methods, and characterization are present below.

Material

A polylactic acid biopolymer (Nature Work PLA Polymer 4032D) with a density of 1.24 g cm^{-3} and a melting point of 170°C was chosen as matrix. A microcrystalline cellulose (MCC) with a mean particle size of 20 μm, supplied in powder form by Sigma Aldrich was used as a raw material. Nanocellulose suspension was procured from Faculty of Forestry, University of Toronto. Acetic anhydride, sodium hydride, and dimethyl formamide were purchased from Sigma Aldrich.

Method

Preparation of Nanocellulose by Acid Hydrolysis. Acid hydrolysis of MCC was performed by standard procedure as mentioned elsewhere (Cranston and Gray, 2006).[22] Hydrolysis was carried out with 64% (w/w) sulphuric acid at 45°C for 45 min with constant stirring. Typically, 40 g of filter aid (dried at 105°C for 30 min) was treated with 700 mL of acid. Immediately following the acid hydrolysis, the suspension was diluted 10-fold with deionized water to quench the reaction. The suspension was centrifuged at 6000 rpm for 10 min to concentrate the cellulose and to remove excess aqueous acid. The resultant precipitate was rinsed, recentrifuged, and dialyzed against water for 5 days until constant neutral pH was achieved. Acid hydrolyzed nanocrystalline cellulose (NCC) was eventually freeze dried to produce a powdered form of the crystals, which was later surface acetylated.

Surface Acetylation of Nanocellulose. In a 1 L round bottom flask, 15 g of freeze dried nanocellulose and 100 mL of dimethyl formamide were stirred at 60°C for half an hour. Sodium Hydride (7 g, 60% dispersion in mineral oil) was added portion wise in the reaction mixture and stirring was continued overnight (16 h) in a nitrogen atmosphere. Next day, acetic anhydride (10 mL) was added and stirred for further 3 h.

The above reaction mixture was cooled to room temperature with continuous stirring. Finally ethanol (50 mL) was added carefully to deactivate excess sodium hydride. The reaction mixture was poured into 400 mL of water and stirred; the solid was collected by filtration and washed with water and acetone, dried at 80°C in a vacuum oven, to give the acetylated nanocellulose (~15 g). Acetylated nanocrystalline cellulose was coded as AC-NCC, while acetylated nanofibrillated cellulose were coded as AC-NFC.

Preparation of Nanocomposites. Composites were prepared by solvent casting technique, using dichloromethane (DCM) as the medium. The desired amount of AC-NCC was added along with 20.0 g of PLA into DCM to produce a mixture. The mixture was then conditioned overnight to eliminate bubbles and was then cast into a petri dish. The DCM was allowed to evaporate at ambient temperature (25°C) for 24 h. Finally the solidified films, with a thickness of around 1 mm, were vacuum

dried overnight, and then kept in a desiccator containing silica gel. Composites with pure cellulose were coded as PLA-AC-NCC.

Characterization

Confirmation of Acetylation by Solid State ^{13}C-NMR. Solid State NMR study was conducted to confirm the surface acetylation of NCC. The CP/MAS ^{13}C-NMR spectra were recorded on a VNMRS 600 MHz NMR spectrometer equipped with 4 mm CPMAS triple resonance probe. The ^{13}C frequency was 150.8 MHz and the chemical shift resonances were referenced to the adamantane chemical shifts obtained with a similar pulse sequence. Acquisition was performed with a CP pulse sequence using a 5.25 ms proton $\pi/2$ excitation pulse, a spectral width of 50 kHz, an acquisition time of 25 ms using a SPINAL-64 decoupling scheme of 70 kHz strength and a 5 s delay between transients. The Hartmann-Hann match was optimized on the 1 sideband at a MAS speed of 8 kHz with a contact time of 500 ms and a linearly ramped-CP field of 30 ± 0.8 kHz. Typically, $12{,}000 - 16{,}000$ transients were accumulated at 25°C. A line broadening of 50 Hz and zero filling to 65 k points were used to process the spectra.

Morphological Studies. The morphology of AC-NCC and AC-NFC was investigated by atomic force micrography (AFM) technique. The images (512 × 512) were recorded using scanning rates of 0.250 Hz. The drive frequency and amplitude was 280.02 Hz and 186.0 mV. AC-NCC and AC-NFC powder were dispersed in distilled water. A drop of the solution was deposited on a silicon wafer and allowed to dry prior to imaging.

Morphology of cryo-sectioned samples of PLA-NFC nanocomposites at different loading of weight percentage ($1 - 5$ wt %) were examined using the FEI Nova Nano SEM (2007) in immersion mode, using the STEM detector, at an acceleration voltage of $15 - 20$ kv. Samples were cryo-sectioned to produce ultra-thin film specimen of 60 nm thick, at 120°C and then placed in a TEM grid. They were then negatively stained by uranyl acetate to produce better contrast in imaging. TEM grids were then mounted in the STEM holder which was then attached to the microscope for imaging. Various sample surfaces were scanned to obtain a visual impression of fiber fracture, distribution, and the appearance of the fiber/polymer interface.

Rheological Measurements. Small amplitude oscillatory shear (SAOS) and steady shear tests were performed using a strain controlled rheometer (ARES-TA Instruments) with parallel plate geometry (25 mm plate diameter) at 170°C under nitrogen atmosphere. Disk-shape samples were positioned in the parallel plate fixture and left for 10 min to minimize any residual stress resulting from sample preparation. The gap was set at 2 mm by gradually squeezing the sample. PLA, PLA-NCC, and PLA-AC-NCC nanocomposites were found to be stable at 170°C for a period of over 2 h. Hence, thermal degradation was considered to be negligible during the rheological measurements.

In SAOS experiments, the linear viscoelastic region was first determined using strain sweep from 0.1 to 100%, at a constant frequency of 10 rad/s. The linear viscoelastic region was identified as the region in which the elastic modulus, G', of the sample experienced less than 5% reduction. Then SAOS tests were conducted in the frequency range of $0.05 - 100$ rad/s at 170°C. The results provided by this test included complex viscosity (η^*), elastic modulus (G') and loss modulus (G''). These parameters provide detailed description of the viscoelastic behavior of the samples.

RESULTS AND DISCUSSION

Acetylation of Nanocrystalline Cellulose

Acetylated NCC was characterized by solid-state cross-polarization magic angle spinning carbon-13 nuclear magnetic resonance (CP/MAS 13C-NMR) spectroscopy. The reaction scheme is shown in Figure 1(a). Figure 1(b) represents the spectral curve by ^{13}C solid state NMR. The two chemical shifts located at 172 ppm and 20 ppm, as assigned to —C═0 and —CH_3 stretching, clearly confirmed that successful acetylation of NFC has been achieved. The results obtained were similar to the observation made by Lin *et al.*,[23] where acetylation was performed on cellulose nanocrystals.

Morphological Study

Figure 2(a,b) show the inherent crystalline structure of acetylated crystalline nanocellulose morphology and formation of nanofibril network in AFM study. It is observed in Figure 2(a), that acid hydrolyzed NCC still retained the rod-like morphology with an aspect ratio of 4 and equivalent volume diameter of ~12.58 nm, as calculated from the micrographs. From the imaging on NFC as revealed in Figure 2(b), it is apparent that the core structure was formed by the internal fibrillation of submicron nanofibrils of $10 - 30$ nm, to several hundred nanometers, which probably resulted from external fibrillation.

In comparison to nonhydrolyzed microcrystalline cellulose, it is certainly evident that there is a subtle particle reduction which eventually leads to reduced agglomeration and improved dispersion of the NCC particles.[21]

A comparative analysis on the state of dispersion of the different nanocomposites at 2.5 wt % is compared, where the cell nucleation and agglomeration starts to appear. The state of dispersion of AC-NCC in PLA is very similar to that of AC-MCC, as reported elsewhere.[21] This is evident from SEM micrograph in Figure 3(a,b). Similar to the previous study, it is observed that cell nucleation with agglomeration starts at 2.5 wt %. Figure 3(c) shows the AC-NFC morphology in the matrix (2.5 wt %), as derived from SEM micrographs in STEM mode. The addition of fillers did not destroy the original structure of PLA. However, with a continuous increase in the loading level of the fillers, as observed in Figure 3(d) (3.5 wt % AC-NCC) and Figure 3(e) (5 wt % AC-NCC), some agglomerates emerged, which is mainly attributed to self-aggregation of the superfluous nanofiller. This result is similar to the study by Fernandes *et al.*[24] and Zepic *et al.*,[25] where the random orientation and the good dispersion of the nanofibrillated cellulose in the chitosan matrices were evident.

Rheological Measurements

The advantage of using rheology as a technique to measure dispersion is that using samples of macroscopic dimension offers an integrated picture of the composite material with increased

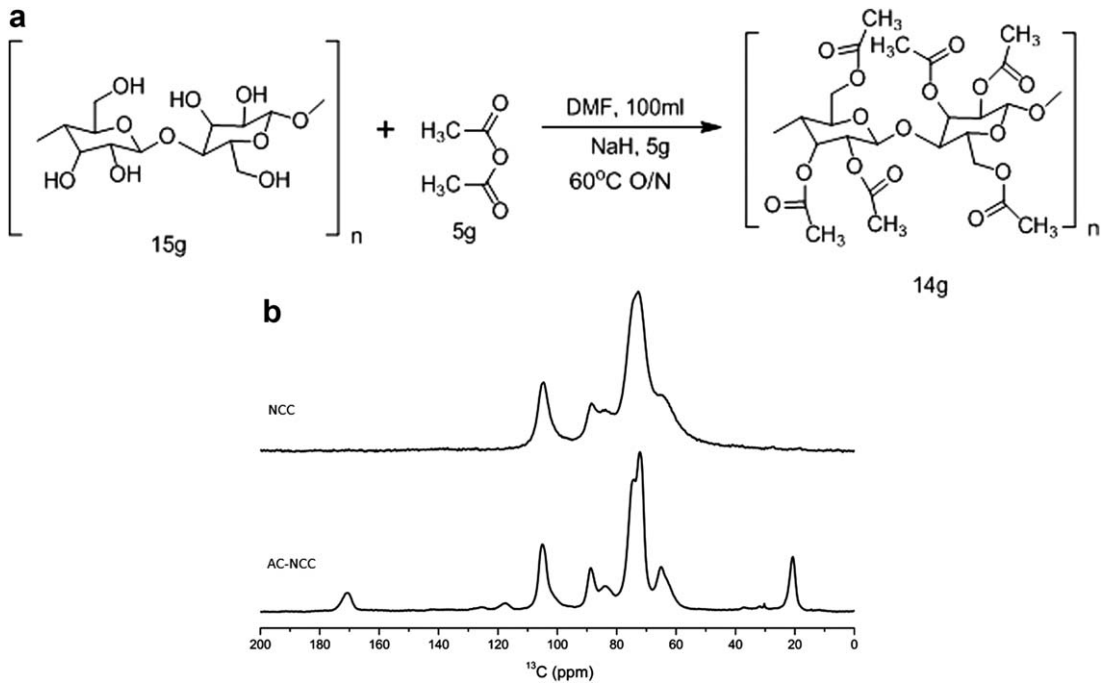

Figure 1. (a) Reaction scheme of acetylation of cellulose. (b) 13 C CP-MAS NMR spectra of pure NCC and acetylated NCC.

data reliability, as compared to other methods using small samples that are prone to micro-scale in homogeneities. Investigation on dispersion, network formation and microstructural changes of AC-NCC in the PLA matrix at melt state is performed by oscillatory measurements in the linear viscoelastic region.

In this study, rheology is envisaged as a tool to assess the quality of dispersion by applying two techniques. They include analyzing the rheological percolation at low frequency moduli and probing to fit the higher frequency data in the Krieger-Dougherty model. Rheological data for different loadings of the filler, as referred before in percentage weight, is now converted to volume fraction, which will help in further analysis of the maximum packing fraction. Thus the new volume fraction of the earlier weight percent (1, 1.5, 1.75, 2.5, 3.5, and 5) corresponds to (0.001, 0.013, 0.015, 0.022, 0.031, and 0.042), respectively. The volume fraction is calculated by using the solid densities of NCC and PLA as 1.25 g cm^{-3} and 1.46 g cm^{-3}, respectively, as available from the technical data sheet and equation (ii) as described below.

$$V_f = \frac{W_f/\rho_f}{\frac{W_f}{\rho_f} + (1 - W_f)/\rho_a} \quad \text{(ii)}$$

Where W_f and ρ_f correspond to the weight fraction and solid density of nanocellulose respectively. ρ_a represents the solid density of neat PLA.

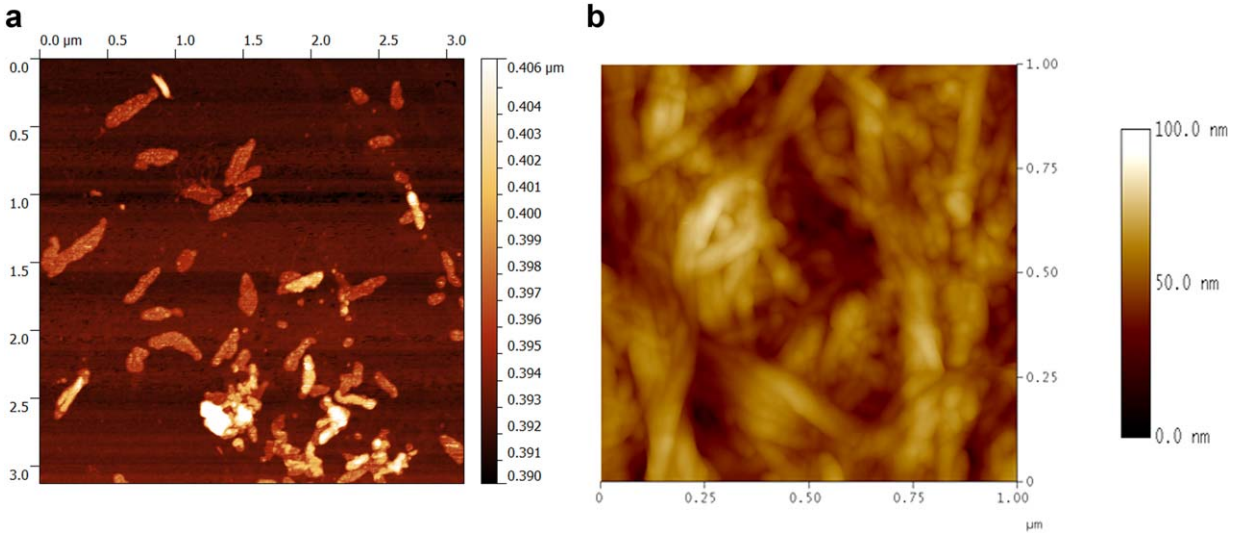

Figure 2. (a) AFM image of nanocrystalline cellulose showing the rod like structure. (b) AFM Image of nanofibrillated cellulose network structure showing the inherent network like structure. [Color figure can be viewed in the online issue, which is available at wileyonlinelibrary.com.]

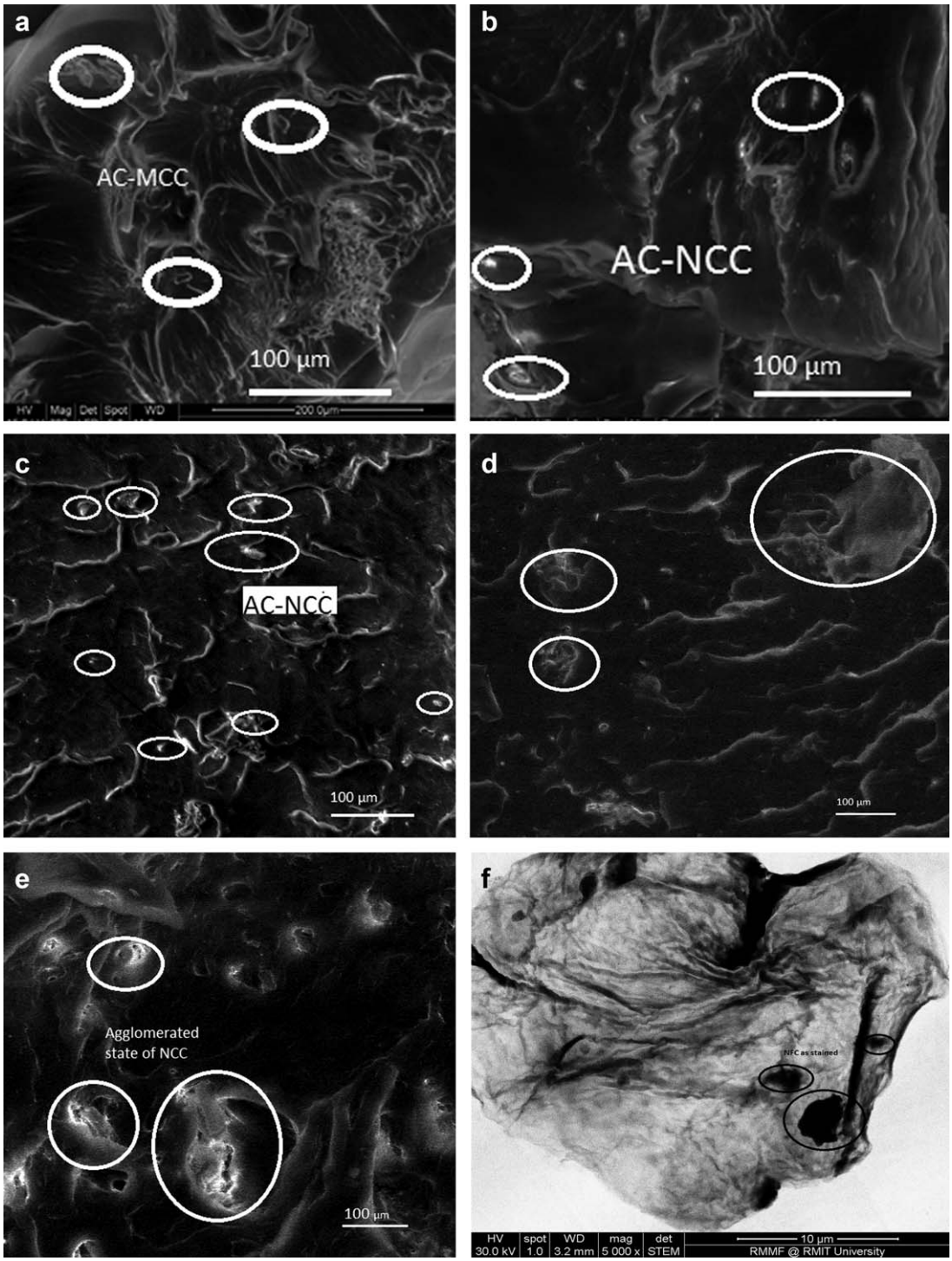

Figure 3. (a). Morphology of PLA-AC-MCC (2.5 wt %) showing a reasonable dispersed state in matrix (b). Morphology of PLA-AC-NCC (1.5 wt %) showing a better homogeneous dispersion state (c). Morphology of PLA-AC-NCC (2.5 wt %) showing an agglomerated state (negatively stained) (d). Morphology of PLA- AC-NCC (3.5 wt %) showing the tendency to agglomerated state (e). Morphology of PLA-AC-NCC (5 wt %) showing the agglomerated state (f) Morphology of PLA-AC-NFC (2.5 wt %) showing the network formation (negatively stained).

Small Angle Oscillation Shear (SAOS) Results. Small angle oscillation shear (SAOS) measurements were carried out to study the rheological behaviour of the polymer systems in light of the microstructural characteristics of AC-NCC. Figure 4(a) shows the results of the storage modulus versus dynamic strain sweep, of PLA-AC-NCC composites of different loadings, used to determine the linear viscoelastic region (LVR). A critical strain Yc was determined at 10 rad/s. Figure 4(b,c) show the storage and loss moduli of the nanocomposite at various loadings (0.008 − 0.04) of volume fraction (∅) at 170°C versus dynamic frequency sweep, respectively.

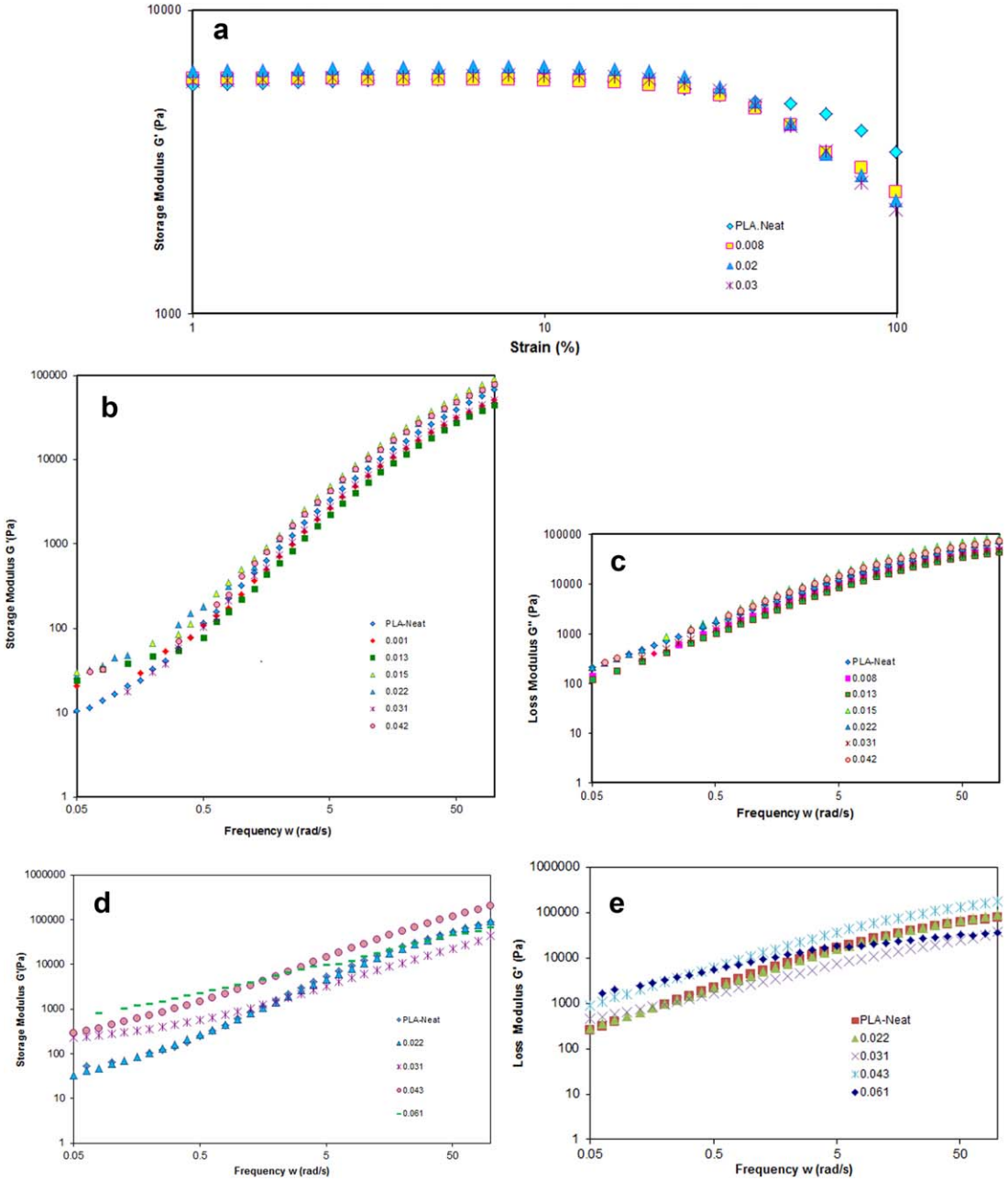

Figure 4. (a) Storage modulus versus dynamic strain sweep test. (b) Storage modulus vs frequency sweep test of PLA-ACC composites (0-0.042 vol fraction). (c) Loss modulus vs dynamic frequency sweep test of PLA-ACC composites (0-0.042 vol fraction). (d) Storage modulus vs dynamic frequency sweep test of PLA-AC-NFC composites (0-0.061 vol fraction). (e) Loss modulus vs dynamic frequency sweep test of PLA-AC-NFC composites (0-0.061). [Color figure can be viewed in the online issue, which is available at wileyonlinelibrary.com.]

The nonlinear regions for PLA matrix were observed to commence around 1.5 wt %. It was also observed that the nonlinear region eventually became shorter with increased loading of the filler. In all dynamic frequency sweep tests, the frequency is varied from 0.05 rad/s to 100 rad/s. In general, the classical viscoelastic behavior of a homogeneous polymer solution/melt is distinguished by $(G'' > G')$, where at low frequency (terminal region) $G'' > \omega^2$ and $G' > \omega$.[27] In general, from the experimental study, it is observed that the PLA sample showed liquid-like behavior at low frequency (G''/G'), where the slopes of G' and G'' were 1.28 and 0.94, respectively. Deviation from the exponent of 2 for loss and 1 for storage moduli could be attributed to the polydispersity of the commercial PLA resin, probably due to the presence of the two lactide forms (L-lactide and D-lactide). From Figure 4(b,c), it is also evident that the enhancement of loss modulus (G'') is more predominant than storage modulus (G') of PLA-AC-NCC composite. It was also observed that at lower frequency range, the nanocomposites behaved more solid like, while at higher frequency range, where the hydrodynamic force is more evident, the composites behaved

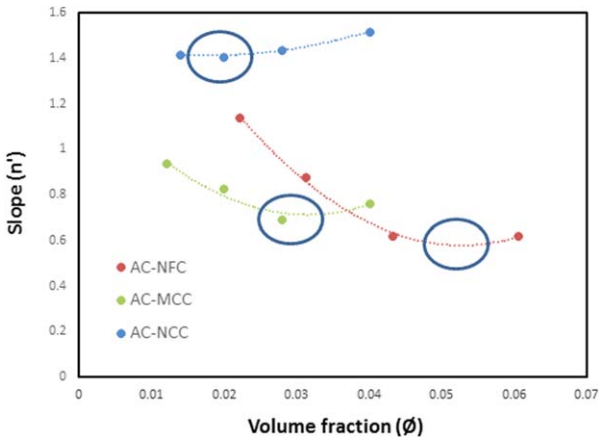

Figure 5. Rheological percolation taking lower frequency data for PLA-AC-MCC, PLA-AC-NCC, and PLA-AC-NFC. [Color figure can be viewed in the online issue, which is available at wileyonlinelibrary.com.]

liquid like. This is similar to the results as reported earlier.[21] It was further observed that at lower frequency, storage modulus was more sensitive to the presence of NCC filler. Similar trend is also observed in case of PLA-AC-NFC composites as shown in Figure 4(d,e).

From Figure 4(d,e), it is also evident that enhancement of storage modulus (G') of PLA-AC-NCC and PLA-AC-NFC composites as compared to neat PLA is significant at all levels of loadings, up to a loading of $\varnothing \sim 0.04$(within the range of $0.008 - 0.04$). Furthermore, it was also observed that the slopes of both loss and storage moduli versus angular frequency in the terminal region were lowered by addition of AC-NCC/AC-NFC to PLA. This is very similar to the previous study, as reported earlier on PLA and acetylated cellulose microcrystals.[21]

Fitting Lower Frequency Data to Rheological Percolation and Scaling Law

Rheological Percolation. Further to the analysis, the slope of G' at lower frequency, which is represented as n', is plotted against various loadings ($\varnothing = 0.008 - 0.04$), of PLA-AC-MCC, PLA-AC-NCC,s and PLA-AC-NFC composites, as shown in Figure 5. This figure evaluate the rheological percolation threshold for a uniform dispersion. From these figures, it is observed that around $\varnothing \sim 0.02 - 0.028$ for PLA-AC-MCC, $\varnothing \sim 0.018 - 0.02$ for PLA-AC-NCC and $\varnothing \sim 0.052$-0.055 for PLA-AC-NFC composites, respectively, a region of minimum slope exists and indicates that beyond that region, dispersion of the nanofiller is affected by agglomeration. This empirical study is used to quantify the degree of dispersion and evaluate the optimal loading for a uniform dispersion of AC-NFC in PLA matrix.

Fitting Higher Frequency Data to the Krieger-Dougherty Equation. In order to calculate the effective hydrodynamic aspect ratio, Ren *et al.*'s[28] expression will be used, which is rewritten in terms of the average aspect ratio of the tactoids (A_f):

$$A_f = \frac{3\varnothing_R}{4\varnothing_{per}} \quad \text{(iii)}$$

Using the percolation threshold volume fraction for randomly packed overlapping spheres ($\varnothing_R = 0.30$)[29] and the experimentally obtained percolation threshold $\varnothing_{per}$ from Figure 5(a,b), the value of $A_f \sim 11.2$ for AC-NCC and $A_f \sim 4.5$ for AC-NFC are obtained. The value obtained here is in line with that obtained from SEM and AFM study in morphology as observed. The difference in the value is indicative of the fact that rheological methods probe an effective "hydrodynamic" aspect ratio.

Further to that study by Vermant *et al.*,[30] an attempt has been made here to fit the higher frequency data to the Krieger-Dougherty equation, as mentioned earlier. Three sets of data, namely the high frequency data set of PLA-AC-NCC and PLA-AC-NFC composites, as available from Figure 4(b,d) respectively, and the high frequency G' data set of acetylated microcrystalline cellulose-based PLA composite (PLA-AC-MCC) from earlier study[21] are fitted to the Krieger-Dougherty equation in Figure 6. In earlier study, as referred to here, cellulose microcrystals were surface acetylated and the reported percolation reached at approximately around a volume fraction of 0.028. Applying the Brenner equation for intrinsic viscosity for oblate spheroids and A_f found from eq. (iii),[31] values of $[\eta] \sim 6.85$, $[\eta] \sim 9.01$ and $[\eta] \sim 4.09$ for AC-MCC, AC-NCC, and AC-NFC were determined, respectively. These values are only approximate. The measured data points at the highest volume fraction deviated. Excluding the deviated data point and fitting the Krieger-Dougherty equation, as shown by the lines in Figure 6, yields an effective maximum packing fraction of $\varnothing_{max} \sim 0.05$, $\varnothing_{max} \sim 0.035$ and $\varnothing_{max} \sim 0.065$ for AC-MCC, AC-NCC, and AC-NFC, respectively. As mentioned earlier, the less value of maximum fraction leads to a better dispersion of the nanofiller, according to the Krieger-Dougherty model. These values give a fair indication that microcrystalline cellulose and nanocrystalline cellulose, when surface acetylated, was better dispersed than that of AC-NFC. It was also observed that acetylated nanocrystalline cellulose was better dispersed than microcrystalline cellulose, as evident from the least value of maximum packing fraction. A comparative analysis on the value of rheological percolation and

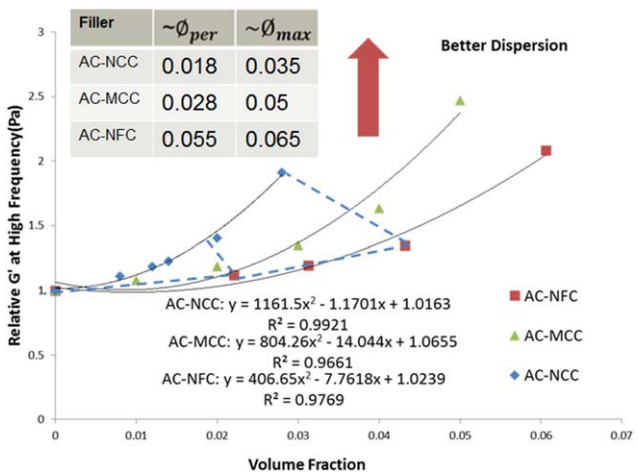

Figure 6. Relative high frequency modulus as a function of volume fraction for AC-NCC/ACMCC/AC-NFC composites. The lines represent the Krieger-Dougherty (KD) equation with a table, where a comparative analysis on percolation value and maximum value packing fraction for different types of cellulosic fillers. [Color figure can be viewed in the online issue, which is available at wileyonlinelibrary.com.]

maximum value packing fraction is shown in the table embedded in the figure. This result is also indicative of the fact that shape and size of the filler is a strong determining factor on the quality of their dispersion in the polymer matrix as reported elsewhere.[32] It can also be suggested that percolation has some phenomenological effect on maximum volume packing fraction (correlation factor ~0.97). For acetylated MCC in earlier study, the percolation reached much early around a volume fraction of $\varnothing \sim 0.028$, whereas in the present case with AC-NCC, the percolation reached at a comparatively lower volume fraction $\varnothing \sim 0.02$, while for AC-NFC, the percolation reached at a comparatively higher value around $\varnothing \sim 0.05$.[21] Similar to the shift in percolation volume fraction value $\varnothing_c$, a shift in maximum volume packing fraction ($\varnothing_{max}$) is also observed. Further analysis on correlation suggests that there exists a strong positive correlation between percolation and maximum value packing fraction. Essentially, maximum packing fraction is the volume occupied by the aggregate, which is dependent on the average particle size. The rheological percolation value again is dependent on the average particle size. So as the average particle size gets reduced due to a better dispersion, the value of percolation decreases, followed by the reduced value of maximum packing fraction. Again from the percolation theory on nanofiller, it is known that the lower the value of $\varnothing_c$, the better the dispersed state of nanofiller.[13] It can thus be concluded that by manipulating the value of $\varnothing_c$, the $\varnothing_{max}$ value can be minimized, which will eventually lead to a better dispersed state of the nanofiller in the polymer matrix.

Discussion on Dispersion and Rheology

Similar to any other nanocomposite research, filler size, loading, and distribution of the reinforcing nanocellulose filler dictate the amount of affected biopolymer, while the surface structure and chemistry of the nanocellulose dictate the intensity of interaction of the particle/biopolymer interphase shape. Morphological study like the conventional microscopy is an effective mean to assess the state of dispersion of the biopolymer matrix. However, the mesoscopic structure is still not understood well with these methods, as they only offer a mean to characterize the local view of the morphology. Rheology plays a significant role in quantifying the state of dispersion in nanocomposite system in mesoscopic scale. Rheological measurements have been used for different types of nanocomposite systems as a complementary tool to monitor the quality of dispersion, primarily in qualitative terms.[30] In this study, a rheological percolation threshold is calculated to quantify the level of dispersion and the optimal loading for a uniform dispersion. Scaling law is applied beyond the percolation value, to probe into the microstructure of the filler that helps eventually in network formation. Moreover, high frequency linear viscoelastic behavior is analyzed and the data is fitted to the Krieger-Dougherty equation to determine the maximum packing fraction.

When the lower frequency data was analyzed by plotting the storage modulus against volume fraction, it is observed that around volume fraction $\varnothing \sim 0.018\text{-}0.02$ for PLA-AC-NCC composites and $\varnothing \sim 0.052 - 0.055$ for PLA-AC-NFC composites, respectively. A region of minimum slope exists and indicates that beyond that region, dispersion of the nanofiller is affected by agglomeration. These values were then used to evaluate the average aspect ratio of the filler in the melt state. Instrinsic viscosity parameters applicable for the Krieger–Dougherty equation were then calculated from the available aspect ratio. When the high frequency data were fitted to the Krieger-Dougherty equation, different values of maximum packing fractions were evaluated as $\varnothing_{max} \sim 0.05$, $\varnothing_{max} \sim 0.035$ and $\varnothing_{max} \sim 0.065$ for AC-MCC, AC-NCC, and AC-NFC, respectively. It was also observed that percolation has some phenomenological effect on maximum volume packing fraction as reflected in Figure 6 (small table provided in the figure).

As observed from the morphological study, MCC and NCC has rod like crystalline structure while NFC has an inter-fibrillated network structure. The rod-like crystalline structure will probably have more chance of forming an organized network in the polymer matrix than that of inherent fibrillated network structure of the NFC filler. This could be one of the reasons as to why the percolation value of AC-MCC and AC-NCC is lower than AC-NFC. Moreover, smaller size of the nanofiller facilitates in better dispersion. This is proved by the lower value of percolation for AC-NCC, in comparison to AC-MCC. Moreover, when scaling law analysis is performed on AC-NCC and the value is compared with standard clay particles, the less value of $d_f \sim 1.06$ suggests a more open fractal structure to form a pronounced network structure, suggesting that in comparison to clay particles, the inherent crystalline structure of AC-NCC helps in forming a more organized network in the PLA matrix.

CONCLUSIONS

Effective surface acetylation on two types of nanocellulose (NCC and NFC) has been achieved by using acetic anhydride and dimethyl formamide. Different types of nanocellulose based (NFC and NCC) PLA nanocomposites were prepared by solvent casting technique. Both microscopy and rheological characterization suggested that acetylated NCC yielded nanocomposites with significantly better dispersion in the PLA matrix. Linear viscoelasticity tests are very sensitive to filler dispersion in the polymer matrix. In general, low frequency rheological characteristics (loss and storage moduli) increased significantly upon adding the nanofiller. A rheological percolation around volume fraction $\varnothing \sim 0.018 - 0.02$ for PLA-AC-NCC composites and $\varnothing \sim 0.052 - 0.055$ for PLA-AC-NFC composites, respectively indicates that AC-NCC was a better candidate for better dispersion, probably of their inherent crystalline rod like structure, that helps them in forming a structured network in the polymer matrix. Different values of maximum packing fractions were evaluated as $\varnothing_{max} \sim 0.05$, $\varnothing_{max} \sim 0.035$ and, $\varnothing_{max} \sim 0.065$ for AC-MCC, AC-NCC, and AC-NFC, respectively. When the high frequency data was fitted to the Krieger-Dougherty equation. The lesser value of the maximum fraction leads to a better dispersion of the nanofiller. A direct correlation between the rheological percolation and maximum packing fraction value was also observed. It was thus concluded the inherent crystalline structure of AC-NCC helps in forming a more organized network in the PLA matrix.

ACKNOWLEDGMENTS

The authors would like to acknowledge the facilities, and the scientific and technical assistance of Prof F. Seperovic for providing us the facility to conduct solid state NMR at Bio21 Molecular Science and Biotechnology Institute, The University of Melbourne; Prof Qipeng Guo and Dr Zhiguang Xu of Deakin University, Mr Phil Francis and Mr Peter Rummel, of the Australian Microscopy and Microanalysis Research Facility at the RMIT Microscopy and Microanalysis Facility, RMIT University; Nadia Zakhartchouk and Frank Antolasic from the School of Applied Sciences; and Mike Allan and Dr Muthu Pannirselvam from the School of Civil, Environmental and Chemical Engineering, RMIT University for their continued support in completing the experimental work.

REFERENCES

1. Weiping, B.; Song, J.; Argyropoulos, D. S.; Lucia, L. A. *J. Appl. Polym. Sci.* **2006**, *100*, 2542.
2. Liang, K.; Gao, Q.; Shi, Q. S. *J. Appl. Polym. Sci.* **2012**, *128*, 1213.
3. Rana, A.; Evitts, R. W. *J Appl. Polym. Sci.* **2014**, *132*, 41807.
4. Mohanty, A. K.; Misra, M.; Hinrichsen, G. *Macromol. Mater. Eng.* **2000**, *276*, 1.
5. Paul, A.; Joseph, K.; Thomas, S. *Compos. Sci. Technol.* **1997**, *57*, 67.
6. Hubbe, M. A.; Rojas, O. J.; Lucia, L. A.; Sain, M. *Bioresources* **2008**, *3*, 929.
7. Siro, I.; Plackett, D. *Cellulose* **2010**, *17*, 459.
8. Moon, R. J.; Martini, A.; Nairn, J.; Simonsen, J.; Youngblood, J. *Chem. Soc. Rev.* **2011**, *40*, 3941.
9. Zimmerman, T.; Bordeanu, N. E.; Shrub, E. *Carb. Polym.* **2010**, *79*, 1086.
10. Zadorecki, P.; Michell, A. J. *Polym. Compos.* **1989**, *10*, 69.
11. Yano, H.; Nakahara, S. J. *Mater. Sci.* **2004**, *39*, 1653
12. Missoum, K.; Belgacem, M. N. J.; Bras, J. *Materials* **2013**, *6*, 1745.
13. Bhattacharya, S. N.; Gupta, R. K.; Kamal, M. R. Polymeric Nanocomposites Theory and Practice; Hanser: Cincinnati, **2008**, p 159.
14. Thostenson, E. T.; Li, C.; Chou, T.-W. *Compos. Sci. Technol.* **2005**, *65*, 491.
15. Jordan, J.; Jacob, K. I.; Tannenbaum, R.; Sharaf, M. A.; Jasuik, I. *Mater. Sci. Eng. A* **2005**, *393*, 1.
16. Barnes, H. A. *Rheo. Rev.* **2003**, *1*, 2003.
17. Stauffer, D. *Pure App. Chem.* **1981**, *538*, 1479.
18. Aranguren, M. I.; Mora, E.; DeGroot, J. V.; Macosko, C. W. *J. Rheol.* **1992**, *36*, 1165.
19. Rueb, C. J. C. F.; Zukoski, C. F. *J. Rheol.* **1997**, *412*, 197.
20. Krieger, I. M. *Adv. Colloid. Interface Sci.* **1972**, *3*, 111.
21. Mukherjee, T.; Sani, M.; Kao, N.; Gupta, R. K.; Quazi, N.; Bhattacharya, S. *Chem. Eng.* **2013**, *101*, 655.
22. Cranston, E. D.; Gray, D. G. *Biomacromolecules* **2006**, *7*, 2522.
23. Lin, N.; Huang, J.; Chang, P. R.; Feng, L.; Yu, J. H. *Carb. Polym.* **2011**, *83*, 23.
24. Fernandes, S. C. M.; Freire, C. S. R.; Silvestre, A. J. D. *Carb. Polym.* **2010**, *81*, 394.
25. Zepic, V.; Fabjan, E. S.; Kasunic, M.; Korosec, R. C.; Hancic, A.; Oven, P. *Holzforschung* **2014**, 68.
26. Mabrouk, A. B.; Magnik, A.; Belgacem, M. N.; Boufi, S. *Compos. Sci. Technol.* **2011**, *71*, 818.
27. Larson, R. G. The Structure and Rheology of Complex Fluids; Oxford University Press: New York, **1998**, p 15.
28. Ren, J. X.; Casanueva, B. F.; Mitchell, C. A.; Krishnamoorti, R. *Macromolecules* **2000**, *33*, 3739.
29. Isichenko, M. B. *Rev. Mod. Phys.* **1992**, *64*, 961.
30. Vermant, J. S.; Ceccia, S.; Dolgovskij, M. K.; Maffetone, P. L. *J. Rheol.* **2007**, *51*, 429.
31. Brenner, H. *Int. J. Multiphase Flow.* **1974**, *1*, 195.
32. Mihut, A. M.; Sánchez-Ferrer, A.; Crassous, J. J. *Polymer* **2013**, *54*, 4194.